Hydrophobic Repacking of the Dimer Interface of Triosephosphate Isomerase by in Silico Design and Directed Evolution[†,‡]

Mariana Peimbert, Lenin Domínguez-Ramírez, and D. Alejandro Fernández-Velasco*

Laboratorio de Fisicoquímica e Ingeniería de Proteínas, Departamento de Bioquímica, Facultad de Medicina, Universidad Nacional Autónoma de México, Apdo. Postal 70-159, 04510 México, DF, Mexico

Received December 20, 2007; Revised Manuscript Received March 10, 2008

ABSTRACT: Triosephosphate isomerase from *Saccharomyces cerevisiae* (wt-TIM) is an obligated homodimer. The interface of wt-TIM is formed by 34 residues. In the native dimer, each monomer buries nearly 2600 Å^2 of accessible surface area (ASA), and 58.4% of the interface ASA is hydrophobic. We determined the thermodynamic and functional consequences of increasing the hydrophobic character of the wt-TIM interface. Mutations were restricted to a cluster of five nonconserved residues located far from the active site. Two different approaches, *in silico* design and directed evolution, were employed. In both methodologies, the obtained proteins were soluble, dimeric, and compact. *In silico*-designed proteins are very stable dimers that bind substrate with a wild-type-like K_m; albeit, they exhibited a very low k_{cat}. Proteins obtained from directed evolution experiments show wild-type-like catalytic activity, while their stability is decreased. Hydrophobic replacements at the interface produced a remarkable shift in the dissociation step. For wt-TIM and for TIMs obtained by directed evolution, dissociation was observed in the first transition, with $C_{1/2}$ values ranging from 0.58 to 0.024 M GdnHCl, whereas for TIMs generated by *in silico* design, dissociation occurred in the last transition, with $C_{1/2}$ values ranging form 3.01 to 3.65 M GdnHCl. For the latter mutants, the stabilization of the interface changed the equilibrium transitions to a novel four-state process with two dimeric intermediates. The change in the intermediate nature suggests that the relative stabilities of different folding units are similar so that subtle alterations in their stability produce a total transformation of the folding pathway.

Oligomeric proteins are central to all biochemical functions. In unicellular organisms such as *Escherichia coli*, oligomers account for 79% of the SWISS-PROT annotated proteins (*1*). The advantages of oligomerization range from fine regulated catalysis and signaling to increased stability and cellular economy (*2*). Two different types of oligomers can be distinguished: obligate or nonobligate. In obligate complexes, the protomers are not found in vivo as stable structures on their own. For these proteins, association is usually coupled to folding (*3, 4*).

All wild-type triosephosphate isomerases (TIMs)[1] studied thus far are obligate oligomers. TIM is the prototype of the $(\beta/\alpha)_8$ barrel, one of the most common folds found in nature (*5, 6*). TIM activity exhibits classical Michaelis−Menten kinetics (*7, 8*). Dimerization is required for catalytic activity and is also essential for TIM stability (*9*−*12*). The three-dimensional structures of oligomeric TIMs from different species are quite similar (*13*−*15*); albeit, different unfolding transitions have been reported: (i) two-state processes for the TIMs from *Bacillus stearothermophilus* (*16*) and rabbit (*17*), (ii) three-state processes involving monomeric intermediates for *Saccharomyces cerevisiae* (henceforth called wt-TIM) (*10, 18*) and *Thermotoga maritima* (*19*), and (iii) four-state processes for *Trypanosoma cruzi* (*20*), *Plasmodium falciparum* (*21*), and *Trypanosoma brucei (22)*. In some of these cases, the unfolding processes are irreversible. For wt-TIM in the presence of GdnHCl, the unfolding−refolding process involves an inactive and expanded monomer with reduced levels of secondary and tertiary structure (*10*). Thermodynamic studies indicate that 70% of the free energy difference between the unfolded monomers and the folded dimer is obtained in the association step (*10*). Moreover, the ΔV_{Unf} values obtained from the pressure-induced unfolding of the intermediate indicate that the monomer is more hydrated than completely folded proteins (*23*). All this evidence demonstrates that the native fold of wt-TIM is acquired after dimerization. The coupling between folding and association must be determined by the properties of the interface.

The TIM interface is mainly formed by the loops located at the C termini of the β strands, and the interaction between monomers is intertwined by loop 3 residues. Catalytic residues K12 and H95 are located in a highly conserved cluster of the interface. The ASA buried upon dimerization is vast, covering 2624 Å^2, and 58.4% of them are hydro-

[†] M.P. received a postdoctoral fellowship from DGAPA-UNAM. This work was partially supported by CONACYT grants (43592, 41328, and 46186-M) and UAM Acuerdos 11 and 13/07 del Rector General. D.A.F.-V. received a summer stay fellowship from ACS-AMC.

[‡] Part of this work was performed during a sabbatical stay of D.A.F.-V. at the Departamento de Ciencias Naturales and Departamento de Química, Universidad Autónoma Metropolitana, Mexico.

* To whom correspondence should be addressed. E-mail: fdaniel@servidor.unam.mx. Telephone: (5255) 56232259. Fax: (5255) 56162419.

[1] Abbreviations: CD, circular dichroism; GdnHCl, guanidinium hydrochloride; SCM, spectral center of mass; TIM, triosephosphate isomerase.

10.1021/bi702502k CCC: $40.75
Published on Web 04/26/2008

phobic. In addition, four salt bridges and several hydrogen bonds stabilize the dimer (*24*).

Hydrophilic contacts stabilize interfaces significantly and provide binding specificity (*25, 26*). Conversely, the magnitude of the buried hydrophobic surface area has been proposed to be directly related to the interaction energy between proteins (*3, 27*−*29*). For obligate oligomers, where association is coupled to folding, the interface can be considered a nucleation site. The role of hydrophobic interactions at obligate interfaces has been addressed in a few studies. For the Arc repressor, Sauer and co-workers observed that the replacement of polar interactions with hydrophobic ones leads to stable homodimers that retain structure and function (*30*). Furthermore, for a triple mutant, a 1250-fold increase in association rate was reported (*31*). Recently, *in silico* design approaches have been used to increase the affinity by increasing the buried hydrophobic area (*32*). In the work presented here, we study the functional and thermodynamic consequences of replacing hydrophilic interactions with hydrophobic ones in TIM folding and association processes. For this purpose, a cluster of interface residues was modified using two approaches, *in silico* design and directed evolution.

MATERIALS AND METHODS

Glycerol-3-phosphate dehydrogenase (GDPH) and GdnHCl were from Boehringer-Mannheim. Restriction enzymes, high-fidelity Vent DNA polymerase, and T4 DNA ligase were purchased from BioLabs. Dithiobis(succinimidylpropionate) (DSP) was from Pierce Chemical Co. All other reagents were purchased from Sigma Chemical Co.

Design and Construction of DesTIMs. For the identification of the wt-TIM interface, a pair of residues was considered part of the interface when the distance to a residue of the other monomer was less than the sum of their corresponding van der Waals radii plus 0.5 Å (*33*). 1YPI (*24*) was used for structural analysis. A cluster of interface residues was selected for design according to their conservation, distance to substrate, and polarity. The residues that meet these criteria are K17, Y46, D48, Q82, and D85. All energy calculations were carried out with Rosetta Design, version 2.0 (*34*). Clashes were removed using repacking and minimization routines. Designs were carried out in the fixed backbone option allowing rigid body displacements between monomers. Substitutions for hydrophobic amino acids at the selected positions were made using the extended rotamer libraries. Interface water molecules were not included. Results with nonidentical sequences in monomers A and B were frequently observed; results with the same sequence in both monomers were selected and analyzed according to the Rosetta energy score "bk_tot". The number of contacts between monomers and electrostatic energy terms were also used as criteria for selection.

The wt-TIM gene was mutated with recursive PCR to produce DesTIMs mutants; these genes were cloned into pET24a (Novagen) using standard molecular techniques, and the constructs were verified by DNA sequencing. Overexpression was carried out in BL21(DE3) pLys cells.

Library and Selection of EvoTIMs. Selection for TIM activity was carried out in a *tpi E. coli* strain (VR101) (*35*), in which the *tpi* gene was interrupted with a kanamicyn resistance cassette; the VR101 strain was a generous gift of G. Saab-Rincón (Instituto de Biotecnología, Universidad Nacional Autónoma de México, Mexico City, Mexico).

The directed evolution library was constructed by recursive PCR. Residues K17, Y46, D48, Q82, and D85 were changed simultaneously by replacing the wild-type codons for N(C/U)C. One microgram of vector was ligated with the mutagenized gene in a 1:3 ratio. The sequence of two clones randomly picked showed that the library was mutagenic for the target residues. Minimal medium (M9) plates, supplemented with ampicillin, kanamycin, and 0.2% glucose, were used for in vivo TIM activity selection. Approximately 10% of the clones grew in <16 h under selective conditions. Six of the faster-growing clones were picked out for sequencing. All of them were mutants; however, some of them did not contain all the target residues mutated. We suppose that these wild-type codons resulted from the selection process and they are not frequent in the library; on the other hand, no extra mutations were found. Overexpression of EvoTIMs was carried out directly in VR101 cells under the *lac* promoter.

Protein Expression and Purification. Cells were grown in LB medium at 37 °C and induced with 0.5 mM IPTG at an OD of 0.4 for 5 h. Purification of TIM mutants was performed as described by Vázquez-Contreras *et al.* (*36*). Briefly, the purification consisted of ammonium sulfate precipitation, followed by exclusion and anionic exchange chromatography steps. Different elution profiles were observed for each mutant in MonoQ chromatography; this excludes contamination from endogenous TIM in the BL21 expression system. All purified fractions exhibit a single band via SDS−PAGE. The concentrations of purified TIMs were measured using the calculated molar absorption coefficient (ϵ_{280}) (*37*). The purity of each mutant was verified by the presence of a single band on the SDS−PAGE gel (data not shown).

Unfolding Experiments. In unfolding experiments, an aliquot of a concentrated TIM solution was diluted in 100 mM triethanolamine (pH 7.4) containing 1 mM EDTA, 0.1 mM dithiothreitol (DTT) (buffer A), and different concentrations of GdnHCl. All samples were measured after incubation for 24 h; this incubation period is sufficient for equilibrium to be attained as evidenced by the lack of change in the fluorescence signal and catalytic activity as well as by the coincidence between the properties of unfolding and refolding samples. TIM mutants were completely unfolded by incubation for 1 h in 5 M GdnHCl. Denaturation was reversible as evidenced by the recovery of native spectroscopic and catalytic properties after GdnHCl dilution.

Chemical Cross-Linking. Proteins were dialyzed against 20 mM KH_2PO_4 (pH 7.4). DSP was resuspended in DMSO at a concentration of 10 mg/mL. Protein and cross-linker were mixed in a 5:1 proportion (w/w). The reaction was stopped after 1 h by the addition of 100 mM Tris-glycine. Results were analyzed by SDS−PAGE.

Spectroscopic Measurements. Fluorescence measurements were made on an ISS (Champaign, IL) PC1 spectrofluorometer. The temperature of the cells was maintained at 25 ± 0.1 °C. Fluorescence measurements were carried out with an excitation wavelength of 280 nm (4 nm bandwidth), and emission was monitored from 300 to 400 nm (4 nm bandwidth). The fluorescence spectral center of mass (SCM) was calculated using the relationship $SCM = \sum \lambda I_\lambda / \sum I_\lambda$. The

circular dichroism of TIM samples was monitored at 222 nm with a JASCO J-715 spectropolarimeter using 0.1 cm path length cells thermostated at 25 ± 0.1 °C. Reference samples without protein were subtracted in all spectroscopic measurements. Thermal unfolding was carried out at scan rates of 0.25 to 1 °C/min.

Catalytic Activity Measurements. TIM activity was measured in 1 mL of a mixture that contained 100 mM triethanolamine, 10 mM EDTA, and 1 mM DTT (pH 7.4) (buffer B), containing 3.0 mM D-glyceraldehyde 3-phosphate, 10 μg of α-glycerolphosphate dehydrogenase (GDPH), 0.2 mM NADH, and 75 pM TIM (*10*). For DesTIMs, 75 nM enzyme was used. Reaction rates were determined from the decrease in absorbance at 340 nm as a function of time in a Beckman DU7500 spectrophotometer with a multicell device thermostatically maintained at 25 ± 0.1 °C. To prevent the effect of denaturants on the activity of GDPH, samples previously used for IF measurements were diluted in <1 min (final GdnHCl concentration of 60 mM for EvoTIMs and 325 mM for DesTIMs).

Hydrodynamic Measurements. Size exclusion chromatography experiments were performed on a Superdex 75 HR 10/30 gel-filtration column coupled to a Pharmacia (Uppsala, Sweden) FPLC system. Protein elution was monitored with a Waters 474 scanning fluorescence detector, using an excitation wavelength of 280 nm (18 nm bandwidth), with emission being monitored at 320 nm (18 nm bandwidth). The incubated enzymes were loaded onto the filtration column, which had been equilibrated with buffer B and GdnHCl. The samples were eluted at a flow rate of 0.4 mL/min. Stokes radii (R_s) values were calculated from elution volumes and a calibration curve (*10, 38*).

Data Fitting. Changes in catalytic activity and fluorescence SCM were normalized using

$$\alpha = \frac{[y(x) - y(x')]}{[y(x=0) - y(x')]} \quad (1)$$

where x' is the denaturant concentration for complete unfolding. Transition midpoints ($C^i_{1/2}$) and slopes ($m^i = 1/d^i$) were obtained by fitting α to sigmoidal Boltzmann equations. For monophasic transitions, the following equation was used.

$$\alpha = \frac{1}{1 + e^{(x - c^1{}_{1/2})/d^1}} \quad (2)$$

For biphasic transitions, a sum of Boltzmann functions was used

$$\alpha = \frac{(1 - A_1)}{1 + e^{(x - c^i{}_{1/2})/d^i}} + \frac{A_1}{1 + e^{(x - C^j{}_{1/2})/d^j)}} \quad (3)$$

where A_1 is the value of α for the plateau region defining the end of the first transition and the beginning of the second one. Data were fitted iteratively using Origin 7.0 (Microcal).

Molecular Dynamics Simulations. For molecular dynamics simulations, the suite GROMACS (*39*) was used. For the simulations of DesTIMs and EvoTIMs, the K17, Y46, D48, Q82, and D85 residues were substituted on 1YPI with the SPDB viewer (*40*). Then, each dimer was independently solvated in a dodecahedral box filled with SPC water molecules and enough counterions to keep the system neutral. The minimal distance from the protein to the boundary of the simulation box was 2.0 nm. Overlapping water molecules were removed when the distance between a solvent atom and a protein atom was smaller than the sum of their van der Waals radii. Energy minimization for the solvent was performed using the steepest descent algorithm for 100 steps. Then, a restrained MD simulation of 100 ps was performed to allow both the protein and the water molecules to relax. During the restrained MD simulation, the protein atoms were harmonically restrained to their position in the crystal with a force constant of 1000 kJ mol^{-1} nm^{-2}. Temperature was controlled via weak coupling to a bath with a constant temperature (T_0 = 300 K; coupling time t_t = 0.1 ps), and the pressure was controlled via weak coupling to a bath with a constant pressure (P_0 = 1 bar; coupling time t_t = 0.5 ps). The production MD run was carried out for 10 ns with the same pressure and temperature coupling constants as for the restrained run. Protein and solvent were coupled to temperature baths separately in the restrained and free MD run. Energy minimization and simulations were performed using periodic boundary conditions. In all simulations, the GROMOS96 53a6 force field was used (*41*); the time step was 2.0 fs, and SHAKE was used for all covalent bonds. The short-range forces (Lennard-Jones and Coulomb) were cut off at 1.0 nm. Long-range forces (Coulomb) were cut off at 1.8 nm and updated during generation of the neighbor list every 20 fs.

For the calculation of accessible surface areas (ASA), 10 snapshots were taken from equilibrated trajectories, and structures were analyzed using NACCESS (*42*). ΔASA was calculated as follows:

$$\Delta ASA = (ASA_{monomerA} + ASA_{monomerB}) - ASA_{dimer}$$

RESULTS

The wt-TIM interface involves 34 residues per monomer; most of them form part of C-terminal loops 1−4 (Table 1). The accessible area buried upon dimerization is quite large (2624 Å^2). To increase the hydrophobic area of the interface, four criteria were used to select the target residues. Residues with more than 95% conservation, <15 Å from the active site, and hydrophobic or those making main chain interactions were discarded. From the nine remaining residues, five were selected because they are clustered in the quaternary structure (Table 1). This cluster, located opposite the active site, is composed of residues K17, Y46, D48, Q82, and D85 (Figure 1). Residues K17 and D48 contribute to the interface with a pair of salt bridges.

Rosetta Designs (DesTIMs). The interface polar cluster [K17, Y46, D48, Q82, and D85 (Figure 1)] was replaced with hydrophobic residues using Rosetta Design (*34*). Rosetta Design searches for rotamer sequences that fit for a given backbone. Sequences are sampled with a Monte Carlo approach and then evaluated with an energy function that includes van der Waals and electrostatic contributions, an implicit solvation model, and statistical terms. In silico designs were selected according to the Rosetta energy parameter "bk_tot". From the best sequences that were obtained, the K17L/Y46F/D48Y/Q82A/D85A (LFYAA) and K17L/Y46F/D48F/Q82F/D85L (LFFFL) mutants were further characterized (see Table 2). LFYAA was designed using all the hydrophobic amino acids, while LFFFL was designed using a more reduced amino acid set comprising only the largest hydrophobic residues (W, F, L, and I). The latter set

Table 1: wt-TIM Interface Residues

secondary structure	residue	informational entropy[a]	identity[b]	distance to substrate[c]
loop C1	10 Asn	3	100% N	Nδ2 4.6
	12 Lys$^+$	2	100% K	Nω 3.5
	13 Leu	43	53% M	N 10.2
	14 Asn	13	98% N	Nδ2 10.1
	15 Gly	38	67% G	N 14.8
	16 Ser	59	36% T	N 18.1
	17 Lys$^+$	78	24% K	N 21.1
loop C2	43 Pro	35	71% P	N 13.5
	44 Ala[d]	63	38% A	N 15.7
	45 Thr	63	29% V	N 18.3
	46 Tyr	55	45% Y	Cδ1 17.6
	48 Asp	82	22% D	N 21.0
loop C3	64 Gln	45	49% Q	Cδ 9.9
	65 Asn	56	46% N	N 12.6
	67 Tyr	81	19% R	N 18.9
	69 Lys$^+$[d]	77	18% R	N 23.7
	70 Ala[d]	78	26% V	Cα 25.6
	71 Ser	66	24% S	N 27.1
	72 Gly	0	100% G	Oε2 28.6
	73 Ala	8	99% A	Oε2 28.5
	74 Phe	34	66% F	Oε2 24.5
	75 Thr	0	100% T	Cα 25.9
	76 Gly	3	99% G	Oε2 20.3
	77 Glu	13	97% E	Oε1 19.2
	78 Asn[d]	44	49% I	Nδ2 16.5
helix 3	79 Ser	13	97% S	N 20.9
	82 Gln	25	75% L	C 22.8
	85 Asp	36	72% M	N 24.6
	86 Val	24	75% L	Cγ2 21.9
loop C4	95 His$^+$	1	100% H	Nε2 3.4
	97 Glu	1	100% E	Oε1 5.4
	98 Arg$^+$	3	99% R	N 9.9
	101 Tyr	52	38% I	N 13.1
	102 Phe	52	50% F	Cδ2 13.3

[a] Informational entropy is inversely proportional to conservation. Data were obtained from the multiple alignment found in HSSP (*63*; http://www.sander.ebi.ac.uk/hssp). [b] Identity percent of the most frequent amino acid at each position, obtained from the HSSP alignment. [c] Shortest distance (angstroms) to C2 of dihydroxyacetone phosphate (PDB entry 1NEY). [d] Interaction only with main chain atoms.

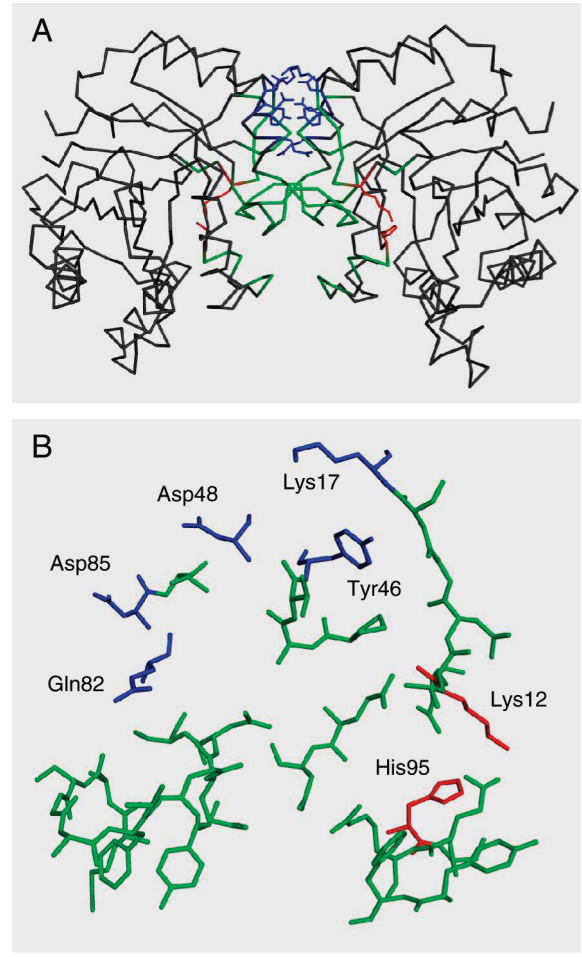

FIGURE 1: wt-TIM structure. (A) The target cluster is represented by blue sticks, while the rest of the interface region is colored green. Active site residues are shown as red sticks. (B) Close-up of one monomer interface residues (sticks) with the same color scheme as in panel A. This figure was generated with Pymol (*62*) using 1YPI.

was picked to maximize the hydrophobic area at the interface. These mutants will be henceforth called DesTIMs.

DesTIMs were constructed and overexpressed as soluble proteins. Both were nativelike as inferred from their CD far-UV spectra (data not shown) and hydrodynamic radii [R_s (Table 2)]. The dimeric nature of DesTIMs was also confirmed by chemical cross-linking with DSP (Supporting Information). The thermal unfolding of DesTIMs and wt-TIM was then studied by CD spectroscopy. As previously reported for wt-TIM (*43*), these enzymes exhibited monophasic and irreversible transitions (Figure 2). CD melts exhibited wt-like cooperativity. The T_{mapp} values of DesTIMs at a scan rate of 1 °C/min (69.8 and 69.9 °C for LFYAA and LFFFL, respectively) were higher than that of wt-TIM (65.8 °C) (Figure 2A). The thermal unfolding of TIM has been shown to be under kinetic control (*43*); therefore, unfolding experiments were carried out at lower scan rates (0.5 and 0.25 °C/min). DesTIMs showed a T_{mapp} ~4 °C higher than that of wt-TIM under all conditions that were tested (Figure 2).

The irreversibility of DesTIM thermal unfolding prompted us to use GdnHCl as an alternative perturbing agent. LFYAA and LFFFL exhibited similar GdnHCl-induced unfolding transitions. These transitions were reversible and at equilibrium (see Materials and Methods). Three transitions were clearly evident in DesTIM unfolding (Figure 3A,B). The first transition, observed by activity measurements, exhibited a $C^1_{1/2}$ close to 1.0 M GdnHCl. The fluorescence spectral center of mass (SCM) remained nativelike up to 2 M GdnHCl. At higher denaturant concentrations, SCM data showed two transitions; the last one ($C^3_{1/2}$) was concentration-dependent (Table 3), indicating that dissociation of a dimeric intermediate occurs in the latest step (Figure 3A,B). This was confirmed by the lack of change in fluorescence anisotropy up to 3 M GdnHCl (data not shown). Analysis by size exclusion chromatography shows an expansion that occurs before dissociation. The latter is accompanied by a decrease in R_s from 2.5 to 3.5 M GdnHCl (Figure 3F). The simplest model that adequately explains SCM, activity, and hydrodynamic data is a four-state model with two dimeric intermediates: 2U ⇆ D ⇆ D* ⇆ N, where D* is an inactive dimeric intermediate with nativelike fluorescence properties and D is also an inactive dimeric intermediate but with a red shift in its fluorescence emission (Figure 3A,B). For DesTIMs, the $C_{1/2}$ values for both activity and fluorescence changes were higher than those of wt-TIM (Table 3). DesTIMs exhibit a very low k_{cat} close to 1 s^{-1}; K_m remained unchanged (Table 2).

Directed Evolution (EvoTIMs). Directed evolution was also used to replace the same interface cluster previously changed by *in silico* design (K17, Y46, D48, Q82, and D85)

Table 2: Comparative Properties of TIM Mutants

	K_m (mM)	k_{cat} (s^{-1})	k_{cat}/K_m (M^{-1} s^{-1})	ΔASA^b (Å^2)	HB ΔASA^b (Å^2)	R_s (Å)
wild type[a]	1.4	6.40×10^3	4.16×10^6	2624 ± 202	1531 ± 8	29.0
LFYAA (DesTIM)	1.26 ± 0.12	1.04 ± 0.04	8.25×10^2	2824 ± 206	1711 ± 131	31.6
LFFFL (DesTIM)	1.2 ± 0.21	0.69 ± 0.05	5.73×10^2	2871 ± 117	1943 ± 85	32.0
PLATA (EvoTIM)	2.44 ± 0.20	$4.16 \times 10^3 \pm 2.2 \times 10^2$	1.64×10^6	2460 ± 194	1546 ± 134	28.6
AFAAS (EvoTIM)	1.09 ± 0.07	$7.02 \times 10^3 \pm 2.1 \times 10^2$	6.44×10^6	2775 ± 96	1727 ± 73	not determined

[a] Data from ref *11*. [b] Calculated from MD trajectories (see Materials and Methods).

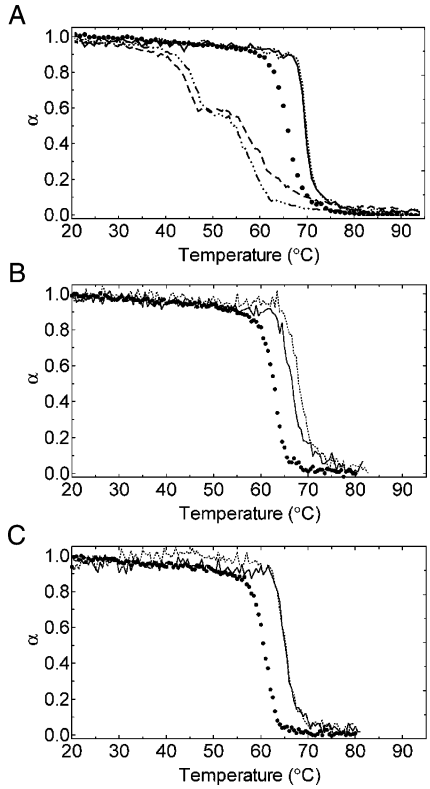

FIGURE 2: Thermal unfolding of TIM mutants followed by CD. Wild-type TIM (●), LFYAA (•••), LFFFL (—), PLATA (---), and AFAAS (-•••-) samples contained 250 μg of TIM per milliliter in 10 mM Tris (pH 7.4). All transitions were irreversible. (A) Scan rate of 1.0 °C/min. T_{mapp} values were 65.8 °C for wt-TIM, 69.8 °C for LFFYA, 69.9 °C for LFFFL, 46.3 and 58.9 °C for AFAAS, and 44.5 and 60.2 °C for PLATA. (B) Scan rate of 0.5 °C/min. T_{mapp} values were 62.6 °C for wt-TIM, 68.1 °C for LFFYA, and 66.5 °C for LFFFL. (C) Scan rate of 0.25 °C/min. T_{mapp} values were 60.6 °C for wt-TIM, 65.2 °C for LFFYA, and 65.1 °C for LFFFL.

by changing simultaneously the wild-type codons for N(C/U)C, which encode some hydrophobic amino acids, namely, A, V, F, I, L, S, T, and P. A library of 4.3×10^4 clones was obtained; the size of the library is bigger than all 8^5 (3.3×10^4) achievable mutants. The library is not big enough to contain all the possible mutations with statistical confidence. Two of the faster-growing clones were selected. The mutant proteins K17P/Y46A/D48L/Q82T/D85A (PLATA) and K17A/Y46A/D48F/Q82A/D85S (AFAAS) were purified for further characterization. These proteins will be termed EvoTIMs.

The k_{cat} and K_m of EvoTIMs were similar to those obtained for the wild-type enzyme (Table 2). EvoTIMs unfolding showed two transitions. The first one is concentration-dependent and correlates with the single transition detected by catalytic activity measurements (Figure 3C,D). Elution profiles of PLATA incubated and eluted at different GdnHCl concentrations showed a decrease in the R_s (Figure 3G). Therefore, as previously reported for wt-TIM, the folding intermediate of EvoTIMs is an inactive monomer. The $C^1_{1/2}$ values for inactivation of EvoTIMs were lower than those of wt-TIM. However, the $C^2_{1/2}$ values for fluorescence changes were slightly higher (Table 3). The thermal unfolding of EvoTIMs was clearly biphasic and showed a remarkable decrease in T_{mapp} (Figure 2A).

DISCUSSION

The folding pattern of DesTIMs is markedly different from that of wt-TIM (Figure 3), where two transitions with a monomeric intermediate were observed (*10*). Changes in T_{mapp} and $C_{1/2}$ for activity and fluorescence SCM changes indicate that DesTIMs are more stable than wt-TIM (Figures 2 and 3 and Table 3). In this respect, the *in silico* design strategy was successful. However, a 10000-fold decrease in k_{cat} was observed (Table 2). It is worth noting that no change in K_m was observed; the preservation of affinity indicates that the interactions responsible for ligand recognition are still in place in DesTIMs. The results obtained from the characterization of the mutants designed with Rosetta showed that the addition of a hydrophobic patch results in dimeric enzymes with high stability and wild-type-like binding affinities but a reduced k_{cat}. To determine if the stability−activity effect of this hydrophobic patch is a general characteristic of this type of interaction, a second approach, i.e., directed evolution, was used to determine if it was possible to design alternative hydrophobic substitutions that retain wild-type K_m and k_{cat} values.

The directed evolution approach produced enzymes with catalytic parameters similar to those obtained for the wild-type TIM (Table 2). Indeed, AFAAS was a bit more efficient than wt-TIM. The unfolding patterns of EvoTIMs and wt-TIM are similar, and these enzymes exhibited two transitions with a monomeric intermediate (Figure 3C−E). When compared with that of wt-TIM, association exhibited a smaller $C_{1/2}$ value (Table 3). The PLATA hydrodynamic profile showed a minimum at 0.3 M GdnHCl, near the $C_{1/2}$ of the first transition. At 0.6 M GdnHCl, where the monomeric intermediate prevails, the R_s returns to the native value, suggesting a denaturant-induced monomer expansion (Figure 3G). These data indicate that in EvoTIMs monomer association was destabilized without altering the general characteristics of the folding pattern and retaining K_m and k_{cat} values.

Catalytic Properties. DesTIMs and EvoTIMs show significant differences regarding catalysis. The binding abilities of all TIM mutants studied in this work remained in the order of magnitude observed for the wild-type enzyme (Table 2). EvoTIMs preserved full catalytic activity; in contrast, the reduced k_{cat} of DesTIMs indicates a perturbation in the fine geometry and dynamics of the catalytic site. To understand

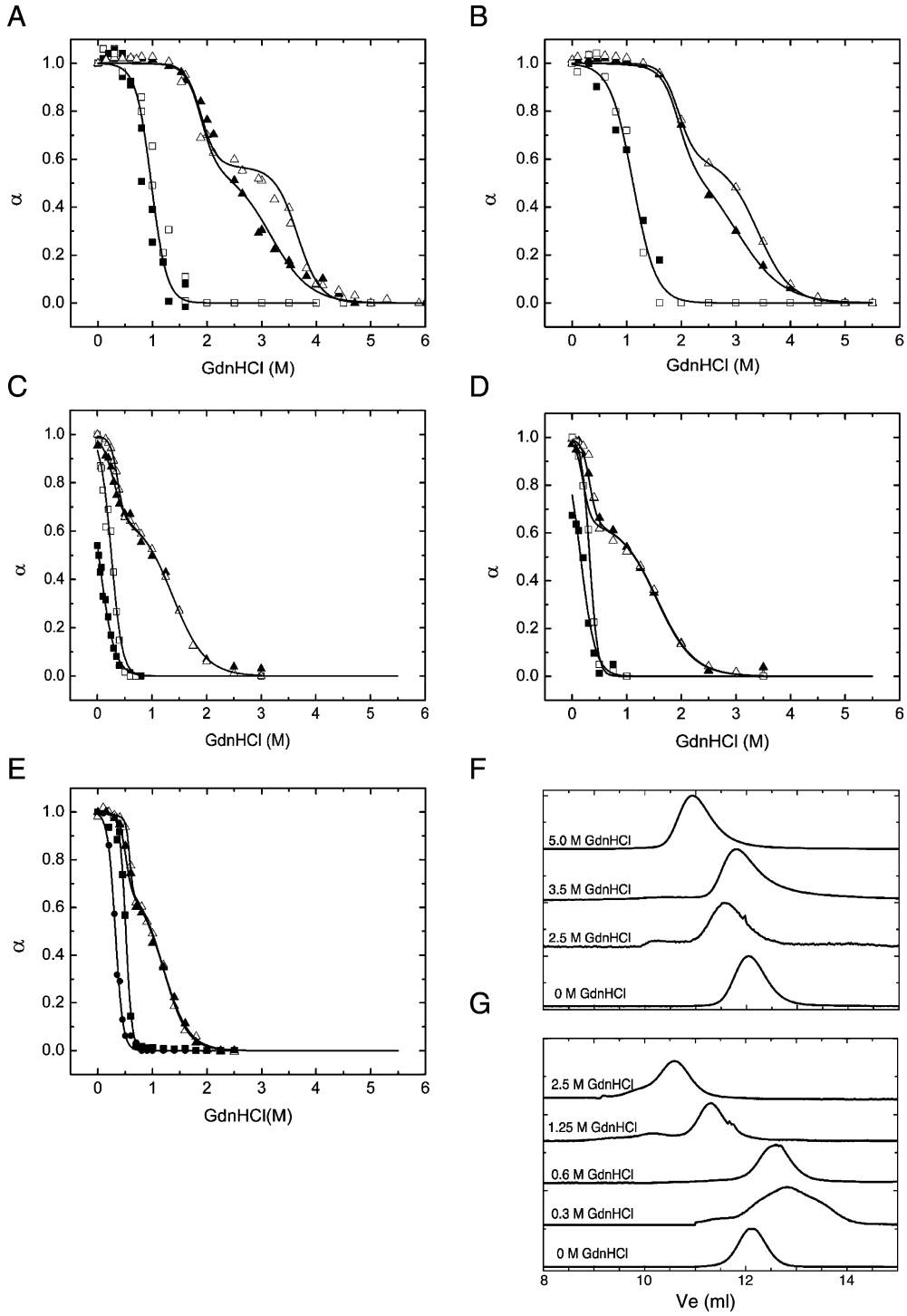

FIGURE 3: GdnHCl-induced unfolding profiles of TIM mutants. Samples were unfolded for 24 h. Thereafter, catalytic activity and spectroscopic and hydrodynamic properties were determined. DesTIM data are shown in panels A, B, and F and EvoTIM data in panels C, D, and G. (A) Catalytic activity [30 (■) and 300 μg/mL (□)] and intrinsic fluorescence [30 (▲) and 300 μg/mL (△)] for LFYAA. (B) Catalytic activity [20 (■) and 200 μg/mL (□)] and intrinsic fluorescence [20 (▲) and 20 μg/mL (△)] for LFFFL. (C) Catalytic activity [50 (■) and 500 μg/mL (□)] and intrinsic fluorescence [50 (▲) and 500 μg/mL (△)] for PLATA. (D) Catalytic activity [15 (■) and 150 μg/mL (□)] and intrinsic fluorescence [15 (▲) and 150 μg/mL (△)] for AFAAS. (E) Catalytic activity [20 (■) and 0.2 μg/mL (●)] and intrinsic fluorescence [20 (▲) and 200 μg/mL (△)] for wt-TIM. (F) Size exclusion chromatography profiles for LFYAA (200 μg/mL). R_s values were 31.6, 34.8, 33.8, and 41.6 Å for 0, 2.5, 3.5, and 5 M GdnHCl, respectively. (G) Size exclusion chromatography profiles for PLATA (200 μg/mL). R_s values were 31.6, 34.8, 33.8, and 41.6 Å for 0, 2.5, 3.5, and 5 M GdnHCl, respectively. Solid lines in panels A−E show fits to the Boltzmann equation (see Materials and Methods).

why DesTIMs are inactive, MD simulations were used to calculate several geometric parameters on EvoTIM and DesTIM models. Global parameters such as total ASA, gyration radius, and secondary structure were indiscernible between wild-type and mutant TIMs (Supporting Information). However, some local parameters behave distinctly; one of them is the dihedral angle formed by the Cα atoms of four active site residues (K12, H95, E165, and S211). The values obtained for the highly active TIMs (18.3 ± 3.2° for wt-TIM, 19.7 ± 2.1° for PLATA, and 19.7 ± 5.3° for

Table 3: Protein Concentration Dependence for GdnHCl-Induced Unfolding of TIM Mutants

		$C^1_{1/2}$[b] (M)	m^{1b} (α M^{-1})	$C^2_{1/2}$[c] (M)	m^{2c} (α M^{-1})	$C^3_{1/2}$[c] (M)	m^{3c} (α M^{-1})
wt-TIM[a]	0.2 μg/mL	0.32 ± 0.004[d]	14.49 ± 0.86[d]	1.19 ± 0.02	4.55 ± 0.23		
	20 μg/mL	0.51 ± 0.004[d]	18.52 ± 1.27[d]	1.19 ± 0.02	4.55 ± 0.23		
	200 μg/mL	0.58 ± 0.003[d]	33.33 ± 3.3[d]	1.19 ± 0.02	4.55 ± 0.23		
LFYAA (DesTIM)	30 μg/mL	0.97 ± 0.01	7.14 ± 0.61	1.89 ± 0.03	7.16 ± 1.43	3.16 ± 0.05	2.79 ± 0.37
	300 μg/mL	0.97 ± 0.01	7.14 ± 0.61	1.89 ± 0.03	7.16 ± 1.43	3.65 ± 0.04	4.81 ± 0.72
LFFFL (DesTIM)	20 μg/mL	1.11 ± 0.02	4.83 ± 0.37	1.95 ± 0.03	6.67 ± 1.47	3.01 ± 0.03	2.38 ± 0.14
	200 μg/mL	1.11 ± 0.02	4.83 ± 0.37	1.95 ± 0.03	6.67 ± 1.47	3.4 ± 0.03	3.33 ± 0.3
PLATA (EvoTIM)	50 μg/mL	0.024 ± 0.005[d]	7.15 ± 0.34[d]	1.37 ± 0.06	3.32 ± 0.44		
	500 μg/mL	0.25 ± 0.01[d]	10.42 ± 1.01[d]	1.37 ± 0.06	3.32 ± 0.44		
AFAAS (EvoTIM)	15 μg/mL	0.15 ± 0.01[d]	7.69 ± 0.95[d]	1.55 ± 0.06	2.96 ± 0.44		
	150 μg/mL	0.32 ± 0.005[d]	14.08 ± 0.79[d]	1.55 ± 0.06	2.96 ± 0.44		

[a] Data from ref *11*. [b] Calculated from activity data (eq 2). [c] Calculated from intrinsic fluorescence data (eq 3). [d] Calculated from activity and intrinsic fluorescence data.

AFAAS) were different from those obtained for DesTIMs (30.7 ± 2.7° for LFYAA and 25.8 ± 4.0° for LFFFL). Since very small perturbations at the active site can have important consequences in catalysis, as shown by the 1000-fold decrease in k_{cat} in the E165D TIM mutant (*44*), we hypothesize that local rearrangements of the active site are responsible for the decrease in k_{cat} observed in DesTIMs. The origin of these geometric perturbations must be traced to the interface. To measure the relative orientation of the two interfacial loop 3 types, another dihedral was defined. This dihedral used S71 and S79 from both subunits. As observed for the active site dihedral, the interfacial dihedral values observed in wt-TIM (174.0 ± 5.9°) were very similar to those of EvoTIMs (179.3 ± 9.8° for PLATA and 177.3 ± 12.2° for AFAAS) and different from those of DesTIMs (152.6 ± 14.3° for LFYAA and 157.6 ± 10.8° for LFFFL). Although MD simulations showed only subtle differences between EvoTIMs and DesTIMs, we proposed that small structural alterations in the cluster formed by residues 17, 46, 48, 82, and 85 are transmitted to loop 3 and the catalytic site. Long-range effects between the interface and the active site have been previously reported (*45*). For thermophilic proteins, low activity values at room temperature have been related to a decreased flexibility, which is a large ΔH^* and a small ΔS^* (*46*). However, we did not observe any sign of a reduced local flexibility in DesTIMs (see the Supporting Information).

Unfolding Patterns. The thermal melt of EvoTIMs exhibited T_{mapp} values lower than those of DesTIMs (Figure 2A). For both the wild type and DesTIMs, a single transition was detected in temperature melts; for example, dimer unfolding, dissociation, and monomer unfolding take place in a single cooperative transition. As previously observed for wt-TIM (*43*), the shift in T_m with different heating rates indicates that unfolding of DesTIMs is kinetically controlled. Nevertheless, at all the scan rates tested in thermal unfolding experiments, T_m values of DesTIMs were higher than those of wt-TIM.

EvoTIM proteins are less stable than wt-TIM, while DesTIMs were more stable. However, both types of mutants exhibited an increase in the estimated buried hydrophobic area when compared with wt-TIM (HB $\Delta\Delta$ASA = 196−411 Å^2). Hence, in the TIM interface, we did not observe a direct relation between stability and buried hydrophobic surface area.

A wide variety of equilibrium folding pathways have been reported for TIM (*10, 16*−*21, 43*). In this work, we have observed two different kinds of transitions; for EvoTIMs, the "wild-type" three-state process with a monomeric intermediate was evident, whereas DesTIMs exhibited a novel four-state process with two dimeric intermediates. The unfolding of EvoTIMs was similar to that observed in wt-TIM; however, in these mutants, the decreased dimer stability makes more evident the three-state character of the folding process. It is noteworthy that for wt-TIM size exclusion chromatography showed an expanded monomer whereas for PLATA a compact monomer that gradually expands was observed. Dissociation of PLATA takes place at low GdnHCl concentrations before substantial monomer expansion is evident. Therefore, the detection of a compact monomeric intermediate in PLATA is a consequence of the decrease in $C_{1/2}$ for dissociation.

Stabilization of the DesTIM interface was expected to result in either the same three-state equilibrium process of wt-TIM, but shifted to higher denaturant concentrations, or the total loss of the intermediate, as observed in temperature melts. Surprisingly, DesTIMs exhibited a completely different GdnHCl-induced unfolding process. The high level of stabilization of the interface gave rise to a four-state model with two dimeric intermediates. This change in the folding transitions suggests that the relative stabilities of different folding motifs are similar so that subtle alterations in their stability produce a total transformation of the equilibrium pathway. A similar behavior, i.e., a change in the folding pathway without gross stability changes, occurs in circularly permuted proteins (*47, 48*).

The replacement of polar interactions with hydrophobic ones produced opposite effects on the stability of the dimer. In EvoTIMs, the dimeric state was destabilized; this indicates that the K17−D48 salt bridge was not compensated by the new hydrophobic interactions. On the other hand, in DesTIMs the dimeric state was stabilized and dissociation was shifted to higher GdnHCl concentrations. A comparison of the unfolding patterns of DesTIMs and EvoTIMs (Figure 3) shows that the dissociation step, i.e., the protein concentration-dependent transition, spans a range of $C_{1/2}$ values from 0.15 M GdnHCl in AFAAS to 3.65 M GdnHCl in LFYAA (Table 3). For all the mutants studied in this work, inactivation takes place in the first transition; therefore, dissociation of EvoTIMs and wt-TIMs was detected by activity changes, whereas for DesTIMs, the bimolecular step was detected by fluorescence changes.

For DesTIMs, the interface was stapled by the new hydrophobic residues. A remarkable consequence of this

interface stabilization was the detection of two dimeric intermediates. Variations of the folding pathway have been previously observed as a result of proline substitutions (*49*), circular permutations (*47, 48*), or the stabilization of particular regions (*50*−*52*). Pathway malleability seems to be a common attribute of TIM and other $(\beta/\alpha)_8$ barrels. Experimental evidence indicates that $(\beta/\alpha)_8$ barrel folding pathways are very diverse. Different β/α units have been proposed to be the primary folding unit (*53*−*58*). With regard to TIM, the number of intermediates and their association state have been found to be specific for each sequence (*11, 13*−*15, 17, 20, 22*). This also holds for the order of β/α unit assembly in the TIM monomer (*59, 60*). Therefore, depending on the particular barrel, the relative stability of β/α units is different; moreover, for each barrel, each β/α unit folds in a more or less cooperative way. It has been suggested that the number of accessible pathways is linked to the number of nucleation motifs (*47, 61*). The possibility of multiple and equivalent nucleation sites arises from the modular architecture of the $(\beta/\alpha)_8$ barrel. In the case of TIM, the interface provides another potential nucleation site. Thus, TIM folding plasticity results from several potential folding units. The substitution of polar interactions with hydrophobic ones at the interface of TIM results in a change in the folding pathway. This suggests that relative stabilities of different nucleation motifs are similar so that subtle alterations produce a change in the number of intermediates and in their association state.

ACKNOWLEDGMENT

We thank D. Baker, O. Furman-Schueler, J. Karanicolas, and members of the Baker lab for suggestions on protein design. We thank Dr. G. Saab for *E. coli* strain VR101. We thank DGSCA-UNAM for the use of the Kan-balam computational facilities.

SUPPORTING INFORMATION AVAILABLE

SDS−PAGE gel of cross-linked DesTIM and analysis of molecular dynamics data (accessible surface area and rmsd). This material is available free of charge via the Internet at http://pubs.acs.org.

REFERENCES

1. Goodsell, D. S., and Olson, A. J. (2000) Structural symmetry and protein function. *Annu. Rev. Biophys. Biomol. Struct. 29*, 105–153.
2. Mei, G., Di Venere, A., Rosato, N., and Finazzi-Agro, A. (2005) The importance of being dimeric. *FEBS J. 272*, 16–27.
3. Jones, S., and Thornton, J. M. (1996) Principles of protein-protein interactions. *Proc. Natl. Acad. Sci. U.S.A. 93*, 13–20.
4. Orengo, C. A., Bray, J. E., Hubbard, T., LoConte, L., and Sillitoe, I. (1999) Analysis and assessment of ab initio three-dimensional prediction, secondary structure, and contacts prediction. *Proteins Suppl. 3*, 149–170.
5. Hegyi, H., and Gerstein, M. (1999) The relationship between protein structure and function: A comprehensive survey with application to the yeast genome. *J. Mol. Biol. 288*, 147–164.
6. Wierenga, R. K. (2001) The TIM-barrel fold: A versatile framework for efficient enzymes. *FEBS Lett. 492*, 193–198.
7. Knowles, J. R. (1991) Enzyme catalysis: Not different, just better. *Nature 350*, 121–124.
8. Knowles, J. R., and Albery, W. J. (1977) Perfection in enzyme catalysis: The energetics of triosephosphate isomerase. *Acc. Chem. Res. 10*, 105–111.
9. Mainfroid, V., Terpstra, P., Beauregard, M., Frere, J. M., Mande, S. C., Hol, W. G., Martial, J. A., and Goraj, K. (1996) Three hTIM mutants that provide new insights on why TIM is a dimer. *J. Mol. Biol. 257*, 441–456.
10. Najera, H., Costas, M., and Fernandez-Velasco, D. A. (2003) Thermodynamic characterization of yeast triosephosphate isomerase refolding: Insights into the interplay between function and stability as reasons for the oligomeric nature of the enzyme. *Biochem. J. 370*, 785–792.
11. Waley, S. G. (1973) Refolding of triose phosphate isomerase. *Biochem. J. 135*, 165–172.
12. Zabori, S., Rudolph, R., and Jaenicke, R. (1980) Folding and association of triose phosphate isomerase from rabbit muscle. *Z. Naturforsch. C35*, 999–1004.
13. Maes, D., Zeelen, J. P., Thanki, N., Beaucamp, N., Alvarez, M., Thi, M. H., Backmann, J., Martial, J. A., Wyns, L., Jaenicke, R., and Wierenga, R. K. (1999) The crystal structure of triosephosphate isomerase (TIM) from *Thermotoga maritima*: A comparative thermostability structural analysis of ten different TIM structures. *Proteins 37*, 441–453.
14. Rodriguez-Romero, A., Hernandez-Santoyo, A., del Pozo Yauner, L., Kornhauser, A., and Fernandez-Velasco, D. A. (2002) Structure and inactivation of triosephosphate isomerase from *Entamoeba histolytica*. *J. Mol. Biol. 322*, 669–675.
15. Wierenga, R. K., Noble, M. E., and Davenport, R. C. (1992) Comparison of the refined crystal structures of liganded and unliganded chicken, yeast and trypanosomal triosephosphate isomerase. *J. Mol. Biol. 224*, 1115–1126.
16. Mainfroid, V., Mande, S. C., Hol, W. G., Martial, J. A., and Goraj, K. (1996) Stabilization of human triosephosphate isomerase by improvement of the stability of individual α-helices in dimeric as well as monomeric forms of the protein. *Biochemistry 35*, 4110–4117.
17. Rietveld, A. W., and Ferreira, S. T. (1998) Kinetics and energetics of subunit dissociation/unfolding of TIM: The importance of oligomerization for conformational persistence and chemical stability of proteins. *Biochemistry 37*, 933–937.
18. Morgan, C. J., Wilkins, D. K., Smith, L. J., Kawata, Y., and Dobson, C. M. (2000) A compact monomeric intermediate identified by NMR in the denaturation of dimeric triose phosphate isomerase. *J. Mol. Biol. 300*, 11–16.
19. Beaucamp, N., Hofmann, A., Kellerer, B., and Jaenicke, R. (1997) Dissection of the gene of the bifunctional PGK-TIM fusion protein from the hyperthermophilic bacterium *Thermotoga maritima*: Design and characterization of the separate triosephosphate isomerase. *Protein Sci. 6*, 2159–2165.
20. Chanez-Cardenas, M. E., Perez-Hernandez, G., Sanchez-Rebollar, B. G., Costas, M., and Vazquez-Contreras, E. (2005) Reversible equilibrium unfolding of triosephosphate isomerase from *Trypanosoma cruzi* in guanidinium hydrochloride involves stable dimeric and monomeric intermediates. *Biochemistry 44*, 10883–10892.
21. Gokhale, R. S., Ray, S. S., Balaram, H., and Balaram, P. (1999) Unfolding of *Plasmodium falciparum* triosephosphate isomerase in urea and guanidinium chloride: Evidence for a novel disulfide exchange reaction in a covalently cross-linked mutant. *Biochemistry 38*, 423–431.
22. Chanez-Cardenas, M. E., Fernandez-Velasco, D. A., Vazquez-Contreras, E., Coria, R., Saab-Rincon, G., and Perez-Montfort, R. (2002) Unfolding of triosephosphate isomerase from *Trypanosoma brucei*: Identification of intermediates and insight into the denaturation pathway using tryptophan mutants. *Arch. Biochem. Biophys. 399*, 117–129.
23. Vazquez-Perez, A. R., and Fernandez-Velasco, D. A. (2007) Pressure and denaturants in the unfolding of triosephosphate isomerase: The monomeric intermediates of the enzymes from *Saccharomyces cerevisiae* and *Entamoeba histolytica*. *Biochemistry 46*, 8624–8633.
24. Lolis, E., Alber, T., Davenport, R. C., Rose, D., Hartman, F. C., and Petsko, G. A. (1990) Structure of yeast triosephosphate isomerase at 1.9-Å resolution. *Biochemistry 29*, 6609–6618.
25. Harbury, P. B., Zhang, T., Kim, P. S., and Alber, T. (1993) A switch between two-, three-, and four-stranded coiled coils in GCN4 leucine zipper mutants. *Science 262*, 1401–1407.
26. Xu, D., Lin, S. L., and Nussinov, R. (1997) Protein binding versus protein folding: The role of hydrophilic bridges in protein associations. *J. Mol. Biol. 265*, 68–84.
27. Janin, J. (1997) The kinetics of protein-protein recognition. *Proteins 28*, 153–161.
28. Tsai, C. J., and Nussinov, R. (1997) Hydrophobic folding units at protein-protein interfaces: Implications to protein folding and to protein-protein association. *Protein Sci. 6*, 1426–1437.

29. Moreira, I. S., Fernandes, P. A., and Ramos, M. J. (2007) Hot spots: A review of the protein-protein interface determinant amino-acid residues. *Proteins 68*, 803–812.
30. Waldburger, C. D., Schildbach, J. F., and Sauer, R. T. (1995) Are buried salt bridges important for protein stability and conformational specificity? *Nat. Struct. Biol. 2*, 122–128.
31. Waldburger, C. D., Jonsson, T., and Sauer, R. T. (1996) Barriers to protein folding: Formation of buried polar interactions is a slow step in acquisition of structure. *Proc. Natl. Acad. Sci. U.S.A. 93*, 2629–2634.
32. Sammond, D. W., Eletr, Z. M., Purbeck, C., Kimple, R. J., Siderovski, D. P., and Kuhlman, B. (2007) Structure-based protocol for identifying mutations that enhance protein-protein binding affinities. *J. Mol. Biol. 371*, 1392–1404.
33. Tsai, C. J., Lin, S. L., Wolfson, H. J., and Nussinov, R. (1996) A dataset of protein-protein interfaces generated with a sequence-order-independent comparison technique. *J. Mol. Biol. 260*, 604–620.
34. Dantas, G., Kuhlman, B., Callender, D., Wong, M., and Baker, D. (2003) A large scale test of computational protein design: Folding and stability of nine completely redesigned globular proteins. *J. Mol. Biol. 332*, 449–460.
35. Saab-Rincon, G., Juarez, V. R., Osuna, J., Sanchez, F., and Soberon, X. (2001) Different strategies to recover the activity of monomeric triosephosphate isomerase by directed evolution. *Protein Eng. 14*, 149–155.
36. Vázquez-Contreras, E., Zubillaga, R., Mendoza-Hernández, G., Costas, M., and Fernández-Velasco, D. A. (2000) Equilibrium unfolding of yeast triosephosphate isomerase: A monomeric intermediate in guanidine-HCl and two-state behavior in urea. *Protein Pept. Lett. 7*, 57–64.
37. Norton, I. L., and Hartman, F. C. (1972) Haloacetol phosphates. A comparative study of the active sites of yeast and muscle triose phosphate isomerase. *Biochemistry 11*, 4435–4441.
38. Uversky, V. N. (1993) Use of fast protein size-exclusion liquid chromatography to study the unfolding of proteins which denature through the molten globule. *Biochemistry 32*, 13288–13298.
39. Lindahl, E. H. B., and van der Spoel, D. (2001) Gromacs 3.0: A package for molecular simulation and trajectory anaysis. *J. Mol. Model. 7*, 306–317.
40. Guex, N., and Peitsch, M. C. (1997) SWISS-MODEL and the Swiss-PdbViewer: An environment for comparative protein modeling. *Electrophoresis 18*, 2714–2723.
41. Oostenbrink, C., Villa, A., Mark, A. E., and van Gunsteren, W. F. (2004) A biomolecular force field based on the free enthalpy of hydration and solvation: The GROMOS force-field parameter sets 53A5 and 53A6. *J. Comput. Chem. 25*, 1656–1676.
42. Hubbard, S. J., and Thornton, J. M. (1993) NACCESS, Department of Biochemistry and Molecular Biology, University College, London.
43. Benitez-Cardoza, C. G., Rojo-Dominguez, A., and Hernandez-Arana, A. (2001) Temperature-induced denaturation and renaturation of triosephosphate isomerase from *Saccharomyces cerevisiae*: Evidence of dimerization coupled to refolding of the thermally unfolded protein. *Biochemistry 40*, 9049–9058.
44. Raines, R. T., Sutton, E. L., Straus, D. R., Gilbert, W., and Knowles, J. R. (1986) Reaction energetics of a mutant triosephosphate isomerase in which the active-site glutamate has been changed to aspartate. *Biochemistry 25*, 7142–7154.
45. Zomosa-Signoret, V., Aguirre-Lopez, B., Hernandez-Alcantara, G., Perez-Montfort, R., de Gomez-Puyou, M. T., and Gomez-Puyou, A. (2007) Crosstalk between the subunits of the homodimeric enzyme triosephosphate isomerase. *Proteins 67*, 75–83.
46. D′Amico, S., Marx, J.-C., Gerday, C., and Feller, G. (2003) Activity-Stability Relationships in Extremophilic Enzymes. *J. Biol. Chem. 278*, 7891–7896.
47. Lindberg, M., Tangrot, J., and Oliveberg, M. (2002) Complete change of the protein folding transition state upon circular permutation. *Nat. Struct. Biol. 9*, 818–822.
48. Martinez, J. C., Viguera, A. R., Berisio, R., Wilmanns, M., Mateo, P. L., Filimonov, V. V., and Serrano, L. (1999) Thermodynamic analysis of α-spectrin SH3 and two of its circular permutants with different loop lengths: Discerning the reasons for rapid folding in proteins. *Biochemistry 38*, 549–559.
49. Wu, Y., and Matthews, C. R. (2002) Parallel channels and rate-limiting steps in complex protein folding reactions: Prolyl isomerization and the α subunit of Trp synthase, a TIM barrel protein. *J. Mol. Biol. 323*, 309–325.
50. Wright, C. F., Lindorff-Larsen, K., Randles, L. G., and Clarke, J. (2003) Parallel protein-unfolding pathways revealed and mapped. *Nat. Struct. Biol. 10*, 658–662.
51. Nauli, S., Kuhlman, B., and Baker, D. (2001) Computer-based redesign of a protein folding pathway. *Nat. Struct. Biol. 8*, 602–605.
52. Friel, C. T., Beddard, G. S., and Radford, S. E. (2004) Switching two-state to three-state kinetics in the helical protein Im9 via the optimisation of stabilising non-native interactions by design. *J. Mol. Biol. 342*, 261–273.
53. Akanuma, S., and Yamagishi, A. (2005) Identification and characterization of key substructures involved in the early folding events of a (β/α)8-barrel protein as studied by experimental and computational methods. *J. Mol. Biol. 353*, 1161–1170.
54. Forsyth, W. R., and Matthews, C. R. (2002) Folding mechanism of indole-3-glycerol phosphate synthase from *Sulfolobus solfataricus*: A test of the conservation of folding mechanisms hypothesis in $(\beta(\alpha))_8$ barrels. *J. Mol. Biol. 320*, 1119–1133.
55. Hocker, B., Beismann-Driemeyer, S., Hettwer, S., Lustig, A., and Sterner, R. (2001) Dissection of a $(\beta\alpha)_8$-barrel enzyme into two folded halves. *Nat. Struct. Biol. 8*, 32–36.
56. Pan, H., and Smith, D. L. (2003) Quaternary structure of aldolase leads to differences in its folding and unfolding intermediates. *Biochemistry 42*, 5713–5721.
57. Zitzewitz, J. A., Gualfetti, P. J., Perkons, I. A., Wasta, S. A., and Matthews, C. R. (1999) Identifying the structural boundaries of independent folding domains in the α subunit of tryptophan synthase, a β/α barrel protein. *Protein Sci. 8*, 1200–1209.
58. Wintrode, P. L., Rojsajjakul, T., Vadrevu, R., Matthews, C. R., and Smith, D. L. (2005) An obligatory intermediate controls the folding of the α-subunit of tryptophan synthase, a TIM barrel protein. *J. Mol. Biol. 347*, 911–919.
59. Pan, H., Raza, A. S., and Smith, D. L. (2004) Equilibrium and kinetic folding of rabbit muscle triosephosphate isomerase by hydrogen exchange mass spectrometry. *J. Mol. Biol. 336*, 1251–1263.
60. Silverman, J. A., and Harbury, P. B. (2002) The equilibrium unfolding pathway of a $(\beta/\alpha)_8$ barrel. *J. Mol. Biol. 324*, 1031–1040.
61. Lindberg, M. O., and Oliveberg, M. (2007) Malleability of protein folding pathways: A simple reason for complex behaviour. *Curr. Opin. Struct. Biol. 17*, 21–29.
62. DeLano, W. L. (2002) The Pymol Molecular Graphics System, DeLano Scientific, San Carlos, CA.
63. Sander, C., and Schneider, R. (1991) Database for homology-derived protein structures and the structural meaning of sequence alignment. *Proteins 9*, 56–68.

BI702502K